Article

Effects of Low Intensity Continuous Ultrasound (LICU) on Mouse Pancreatic Tumor Explants

Despina Bazou [1], Nir Maimon [1], Lance L. Munn [1] (ID) **and Iciar Gonzalez [2,***

[1] Edwin L. Steele Laboratory, Department of Radiation Oncology, Massachusetts General Hospital, Harvard Medical School, 100 Blossom Street, Boston, MA 02114, USA; despinabazou@yahoo.com (D.B.); nmaimon@steele.mgh.harvard.edu (N.M.); munn@steele.mgh.harvard.edu (L.L.M.)

[2] Institute of Physics and Information Technologies, Group of Ultrasonic Resonators, CSIC, Serrano 144, 28006 Madrid, Spain

* Correspondence: iciar.gonzalez@csic.es

Abstract: This paper describes the effects of low intensity continuous ultrasound (LICU) on the inflammatory response of mouse pancreatic tumor explants. While there are many reports focusing on the application of low-intensity pulsed ultrasound (LIPUS) on cell cultures and tissues, the effects of continuous oscillations on biological tissues have never been investigated. Here we present an exploratory study of the effects induced by LICU on mouse pancreatic tumor explants. We show that LICU causes significant upregulation of IFN-γ, IL-1β, and TNF-α on tumor explants. No detectable effects were observed on tumor vasculature or collagen I deposition, while thermal and mechanical effects were not apparent. Tumor explants responded as a single unit to acoustic waves, with spatial pressure variations smaller than their size.

Keywords: low-intensity continuous ultrasound; bioeffects; inflammation; tumor; interferon-γ interleukins; tumor necrosis factor-α (TNF-α); collagen I; vasculature

1. Introduction

Low-Intensity Pulsed Ultrasound (LIPUS) is widely used as an imaging tool in medicine at low intensities (<3 W/cm^2). It is a non-invasive and safe technique used extensively as a diagnostic and therapeutic tool [1–5]. In regular clinical applications, the intensity of the ultrasound applied ranges from about 0.03–1.0 W/cm^2. LIPUS based on contrast-agents has been also applied for imaging [6,7], with high efficiency results at frequencies ranging from 500 kHz and 2 MHz. Different intensities of exposure have been used in the literature for therapeutic purposes such as healing of bone-fracture or soft-tissue lesions, with dosages up to 2 W/cm^2 without tissue damage, and frequencies between 0.7 and 3.0 MHz. Various studies have reported LIPUS-induced cell growth with proliferation and promotion of multi-lineage differentiation with cell expansion and differentiation in tissue culture, including gingival cells [8,9], periodontal cells [10–12], cementoblastic cells [13,14], chondrocytes [15,16] or mesenchymal stem cells [17,18]. Also, LIPUS effects on osteoblasts and enhancement of angiogenesis [19,20] were reported. Some studies showed that LIPUS enhanced cell expansion and differentiation in tissue culture [10,21,22]. However, the underlying molecular mechanisms governing these LIPUS-induced effects on tissues and cells [4,5] still need to be investigated. In addition, LIPUS effects on tumor samples have not been extensively investigated.

All these studies describe the use of conventional pulsed wave generators, typically used for diagnosis methods, to know possible therapeutic effects in cells and tissues. They assume the advantages of non-heating effects on the tissues due to these ultrasonic actuators and the time-gaps between consecutive wave trains.

However, cellular responses to low-intensity US are parameter-dependent, especially in the case of low-intensity pulsed US. Very few studies have reported the influence of LIPUS treatment on the effects induced in bio-samples, including the intensity of the acoustic wave and the pulse repetition frequency [23–25] at frequencies close to 1 MHz. In particular, Chunmei et al. [25] recently investigated (2016) the systematic effects of low-intensity pulsed US on the proliferation of HepG2 and 3T3 cells in vitro by changing the intensity in the range of 0–1.2 W/cm^2, PRF (1 and 100 Hz), and the duty cycle (10%, 20%, and 50%) with a 1.06 MHz generator. They found increased cell proliferation at intensities between 0.4 W/cm^2 and 0.8 W/cm^2 and PRF ~ 100 Hz, but higher intensities generated cell death, while lower pulse repetition frequencies did not induce any detectable effect on the cells. This recent study evidenced the need to know how the duty cycle affects the sample response.

It is a challenge to know the ultrasound effects by elongating the pulse repetition frequency until reaching a limit condition of duty cycle of 100%, at which the distance between consecutive wave trains disappears and the pulsed wave becomes a continuous wave. This challenge led us to perform the current study.

In this paper, we have replaced pulsed waves with continuous low intensity waves at similar frequency and intensity amplitudes. Hereafter, they will be referred to as Low-Intensity Continuous Ultrasound (LICU). LICU maintains the cell vibration throughout the whole acoustic treatment, instead of the intermittent oscillations induced by LIPUS with temporal gaps relaxing the cell oscillatory motion. Thus, the limit condition of an infinite wave-train length was assumed for the continuous wave used in our experiments.

Inflammation is critical for tumor progression. Many cancers arise in sites of infection, chronic irritation, and inflammation. In addition, tumor cells have co-opted some of the signaling molecules of the innate immune system, such as selectins, chemokines, and their receptors for invasion, migration, and metastasis [26]. Hence, the establishment of a new technique that promotes a pro-inflammatory response on tumors for future optimized therapies is of great interest.

We present, for the first time, an exploratory study of the effects of LICU on the inflammatory response of mouse pancreatic tumor explants. We also present a description of the mechanical, thermal, and molecular effects induced by LICU on these explants. We show that LICU causes significant upregulation of IFN-γ, IL-1β, and TNF-α in pancreatic tumor explants. Furthermore, we assess the LICU effects on tumor vasculature and collagen I deposition. We show that LICU is minimally invasive to the tissues' structure and morphology.

2. Materials and Methods

2.1. Ultrasound Exposure System: Chamber of Acoustic Actuation

Our experiments were performed in a small ultrasound exposure system consisting of an open glass chamber of cylindrical geometry (Figure 1A—inner diameter of 10 mm, wall thickness of 1 mm, and height of 4 mm) resonating at f ~ 1 MHz. It was activated by an ultrasonic actuator attached also to the glass slide at a very short distance of 3 mm (Figure 1A): a piezoelectric ceramic Ferroperm pz26 of rectangular area (30 mm × 15 mm × 1.5 mm) resonating in its thickness mode at a frequency f = 1.009 MHz. Both, the chamber and piezoelectric actuator were mechanically connected through the glass slide, thus allowing for the transmission of the ultrasonic vibrations from the piezoelectric ceramic. The chamber was actuated at intensity levels close to 0.1 Watt/cm^2, significantly lower than a tissue injury threshold described in the literature for average intensities up to 30 kW/cm^2 and with a duration of 10 min [27]. At a frequency f = 1.09 MHz, a complex 2D acoustic pressure pattern was established inside the chamber filled with liquid (with a 3 mm-height), with maximal amplitudes of 0.29 MPa (dark areas in Figure 1B) and pressure nodes (bright areas in Figure 1B) separated at distances smaller than 1 mm. Different pressure amplitudes were thus exerted on different parts of the tumor explants within the chamber of treatment.
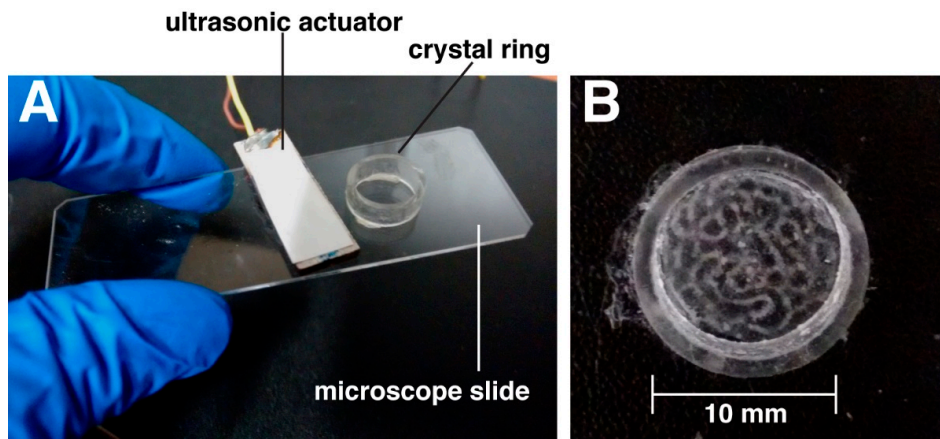
Figure 1. (**A**) Photograph of the ultrasound exposure system. A cylindrical open chamber was formed using a crystal ring (with an inner diameter of 10 mm, wall thickness 1 mm, height 4 mm) glued onto a microscope slide. The cavity was activated by an ultrasonic actuator; a small piezoelectric ceramic Ferroperm pz26 of rectangular area (30 mm × 15 mm × 1.5 mm), resonant at a frequency close to 1 MHz, was placed also on the microscope slide and close to the chamber of treatment. (**B**) 3D acoustic pressure pattern formed inside the acoustic cavity when a continuous wave at f = 1009 kHz (resonance frequency) and a fixed voltage of $V_{P\text{-}P}$ = 10 V is applied.

2.2. Pressure Amplitude Measurements

The acoustic pressure amplitudes inside the acoustic chamber were measured with a high sensitivity (-211 dB re 1 V/µPa) needle hydrophone (Precision Acoustics LTD, Dorchester, UK, SN 1423, Φ = 0.2 mm PVDF) calibrated over the frequency range of 500 kHz to 20 MHz. The probes plug into a submersible preamplifier SN (PA 08072) with a 50 Ω output impedance to reduce the susceptibility to electromagnetic interference, thus allowing very long coaxial cable extensions whilst maintaining a nominal 8 dB voltage gain. The instantaneous pressure (P) was calculated from acquired voltage readings, taking into account the hydrophone sensitivity at the acoustic working frequency (AWF) [28].

A complex pressure pattern was established inside the acoustic chamber at a frequency of 1.009 MHz, as shown in Figure 1B (filmed on aqueous suspension of polystyrene micron-sized particles). This pressure pattern presents spatial variations that include dark areas with maximal pressure amplitudes (of 0.29 MPa) and bright areas with pressure nodes where the particles collect.

In most soft tissue interfaces only a small fraction of the pulse is reflected. The impedance of the pancreas Z_{panc} ~ 1.70×10^6 kg/m^2 s [28] is close to that of the liquid in which is immersed (Z_{liquid} ~ 1.66×10^6 kg/m^2 s), thus providing a very low reflectivity at the interface: $R = \left(\frac{Z_{pancreas} - Z_{medium}}{Z_{pancreas} + Z_{medium}} \right)^2$ ~ $3 \times 10^{-3} \ll 1$. A very small fraction of the pulse is reflected at their interface, so that the pressure pattern within the chamber remained practically unaltered when the tumor sample was introduced.

An average intensity amplitude of I = 0.1 Watt/cm^2 was determined from the pressure amplitude taking into account the size of the chamber that has a surface S ~ 0.4 cm^2. The intensity I of the acoustic wave is proportional to the square power of the pressure amplitude P_0 of the incident wave:

$$I = P_0^2 / 2Z \tag{1}$$

2.3. Attenuation of the Ultrasounds on the Samples

The attenuation inside the chamber is negligible due to its size. In fact, minimal variations of the pressure amplitude measurements were detected by the needle hydrophone within a maximum pressure location.

The attenuation inside the tissue depends linearly on the ultrasound frequency and increases with the sample volume. In our experiments it can be considered negligible due to the small size of the tissue samples (thickness of 1 mm), which are much smaller than any organ, such as liver or kidney, for which authors like Nightingale or Yarmolenko [27,29] reported acoustic attenuation of $\alpha \sim$ 0.3–1 dB/MHz^{-1} cm^{-1}. An injury threshold for organs exposed to ultrasounds has been reported in the literature for average intensities: up to 30 kW/cm^2 for a total duration of 10 min is safe in organs such as kidneys. A spatial peak intensity threshold of 16,620 W/cm^2 was needed before a statistically significant portion of the samples showed injury. This is nearly seven times the 2400 W/cm^2 maximum output of the clinical prototype used to move kidney stones effectively in pigs and more than 30 times the intensity generated in our acoustic resonator. Our experiments were performed at intensity levels significantly lower than this tissue injury threshold.

2.4. Thermal Measurements within the Acoustic Chamber

Ultrasound application can induce some degree of heating. As the energy within the sound wave passes down into the tissues, it causes molecular oscillations in the tissue that can result in heat generation. The rate at which the temperature rises in tissues exposed to the ultrasound linearly depends on the intensity of the acoustic wave *I* and the degree of absorption within the sample (defined through the acoustic attenuation coefficient of the sample α), and is inversely proportional to the tissue density ρ and specific heat C_m [30]:

$$T = \frac{2a \cdot I \cdot t}{C_v} + T_0 \tag{2}$$

where T_0 is the initial temperature of the sample before the actuation of the ultrasound, and *t* is the time of treatment. C_m is close to ~3600 J/(kg K)~4.18 J/cm^3 °C for biological tissues. In our experiments, a thermocouple (Fluke 179 True RMS Multimeter, Norfolk, UK equipped with an adapter Fluke Type K 80 AK-A, Norfolk, UK) was used to measure the spatial temperature inside the acoustic treatment chamber over a period of 2 h.

2.5. Tumor Explant Preparation

The Massachusetts General Hospital Subcommittee on Research Animal Care approved all mouse experiments. Human pancreatic (PANC-1) tumors were grown orthotopically in 8-week-old severe combined immunodeficient mice (SCID) females. Tumors were grown in the mice until they reached 4–5 mm diameter. At this size, necrosis is minimal, but the tumors are large enough to allow multiple, relatively homogenous tumor fragments to be generated from a single tumor. Tumors were then resected and cut into fragments of equal area and thickness of 1 mm and placed into the acoustic chamber in Dulbecco's Modified Eagle's Medium (DMEM). Tumor explants were exposed LICU for 120 min, while explants in the resonator without LICU application served as controls. All experiments were performed in triplicate (i.e., from 3 different mice).

2.6. Immunofluorescence Staining of PANC-1 Tumor Explants

The ultrasound-treated and control PANC-1 tumor explants were fixed, permeabilized, and serum-blocked as per standard procedures. They were then labelled with CD31 (1:100, Millipore, Taunton, MA, USA) and Collagen I (1:500. AbCAM, Cambridge, MA, USA) overnight at 4 °C. Appropriate, fluorescently labelled secondary antibodies were applied for 60 min and washed three times with saline. Cell nuclei were stained with DAPI nuclear stain (Invitrogen, Waltham, MA, USA, 1:200) and washed three more times with saline prior to confocal microscopy.

2.7. ELISAs for Inflammation

The V-PLEX Proinflammatory Panel 1 (human) ELISA Kit (Meso Scale Discovery, Rockville, MD, USA) was used to assay cytokine release following ultrasound exposure. Culture media was collected from control PANC-1 tumor explants (No US) and from explants exposed to 120 min of US.

The Proinflammatory Panel 1 measures the following cytokines, which are important in inflammation response and immune system regulation: IFN-γ, IL-10, IL-12, IL-1β, IL-2, IL-4, IL-5, IL-6, and TNF-α.

2.8. Image Acquisition

Bright field and fluorescence images were acquired with a Nikon SMZ1500 stereomicroscope (Nikon Instruments Inc., Melville, NY, USA) equipped with a Nikon D90 SLR camera and a QIClickTM digital CCD camera (QImaging, Surrey, BC, Canada). Confocal fluorescence images were acquired with an Olympus IX81 microscope ($20\times$ air lens) equipped with the Fluoview software. Slice thickness varied between 1 mm and 5 mm. Projections of confocal images were produced using Image J (NIH, Bethesda, MA, USA).

2.9. Statistical Analysis

The data are shown as mean $\pm$ SEM. Data are normalised relative to control, non-ultrasound treated samples. Analysis of means was performed with a one-way analysis of variance (ANOVA) (GraphPad Prism software, La Jolla, CA, USA). Differences were considered significant at p values less than 0.05. ****: $p < 0.00005$; ***: $p < 0.0005$; **: $p < 0.005$; *: $p < 0.05$.

3. Results and Discussion

Our experiments were performed at intensity levels significantly lower than a tissue injury threshold: average intensities up to 30 kW/cm^2 for a total duration of 10 min are safe in organs such as kidneys [27], and a spatial peak intensity threshold of 16,620 W/cm^2 was needed before a statistically significant portion of the samples showed injury. This is nearly seven times the 2400 W/cm^2 maximum output of a clinical prototype used to move kidney stones effectively in pigs and more than 30 times the intensity generated in our acoustic resonator.

3.1. Mechanical and Thermal Effects on the Samples

In our experiments, tumor explants displayed no apparent motion or deformation under LICU but remained dynamically stable. This is a typical effect caused by high intensity focused ultrasound (HIFU), which can lead to the destruction of the normal tissue.

In our experiments, a temperature rise of 1.0 °C was detected following two hours of acoustic application (Table 1) at room temperature (20 °C). Such temperature rise represents an increase of 5% over its initial value and is approximately six times smaller than that found by Draper et al. [31,32] in muscle tissues exposed to focused waves. They reported a temperature increase of 5.8 °C at 0.8 and 1.6 cm tissue depths after 20 min of ultrasound application (f = 3 MHz and I = 1 W/cm^2), and a 6 °C rise following 120 s of exposure to focused LIPUS on brain tissue. The thermal effects on the tumor explants exposed to LICU can thus be considered negligible.

Table 1. Temperature measurements inside the treatment chamber at different ultrasound application times.

Time of Ultrasound Application (min)	Temperature (°C)
0	20.1
5	20.2
10	20.2
30	20.3
60	20.6
120	21.1

3.2. LICU Effects on Cytokine Secretion, Tumor Vasculature, and Collagen I Production

The results of the cytokine array (Figure 2) showed that after LICU stimulation, IFN-γ, was significantly upregulated by 3-fold compared to control, non-LICU-treated samples. In addition, IL1-β was significantly upregulated by 16-fold, while TNF-α was upregulated 17-fold compared to control, non LICU-treated samples (Figure 2). In contrast, IL-10, IL-12, IL-2, IL-4, IL-5, and IL-6 did not significantly increase following LICU treatment. Cytokines are particularly important in the neoplastic initiation; they are aberrantly produced by tumor cells, macrophages, and other phagocytic cells. In pancreatic cancer, various signaling pathways are perturbed, and this not only affects the tumor cells directly but also influences the stromal cells within and around the tumor [32]. In particular, NF-κB signaling is commonly deregulated in PDAC [33]. A major activator of NF-κB is the cytokine tumor necrosis factor (TNF), which is mainly produced by activated immune cells, especially macrophages and T cells, but can also be expressed by tumor cells [34]. However, the role of TNF in pancreatic tumor progression still remains controversial. While some studies demonstrated anti-tumorigenic properties of TNF [35,36], others have shown the opposite results [37,38]. The 17-fold increase, in TNF-α following LICU thus remains to be further explored.
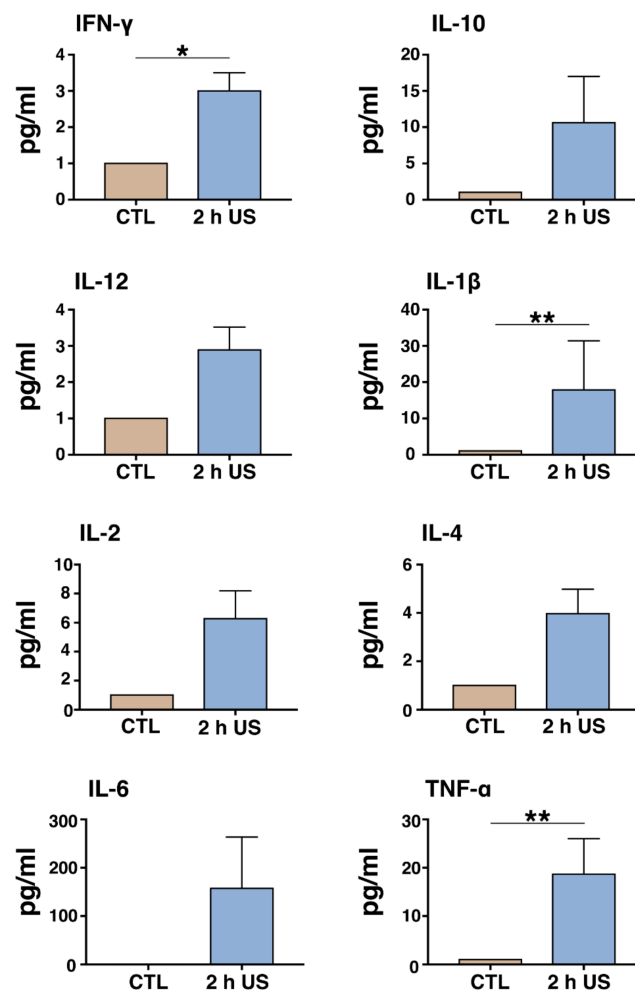

Figure 2. Enzyme linked immunosorbent assay (ELISA) results of the V-PLEX Proinflammatory panel 1. IFN-γ was significantly upregulated 3-fold; IL-β was significantly upregulated by 16-fold, while TNF-α was upregulated 17-fold compared to control, non-low intensity continuous ultrasound (LICU)-treated samples. IL-10, IL-12, IL-2, IL-4, IL-5, and IL-6 did not significantly increase following LICU treatment. **: $p < 0.005$; *: $p < 0.05$.

One of the key features of pancreatic cancer is extended fibrosis, which has been linked to the activation of pancreatic stellate cells (PSCs) [39]. The desmoplastic reaction not only accompanies the disease but plays an active role in its progression and reduces the efficiency of cytostatic drugs [40,41]. Interferon-γ (IFNγ) has been shown to inhibit fibrogenesis by targeting PSCs [42], and thus it has been proposed as an active component for the treatment of pancreatic cancer as part of a chemoradiation protocol [43,44]. Here, we report on a 3-fold increase in IFNγ, suggesting that LICU localized application could be employed as a method to enhance the anti-fibrotic and anti-proliferative effect of IFNγ.

We also demonstrate a significant increase in IL-1β secretion. High plasma IL-1β levels are associated with a significantly increased risk of cancer, and tumor patients with high IL-1 expression have worse prognosis [45]. IL-1 is a key modulator for induction of innate immunity and inflammation and is a major pathogenic mediator of autoimmune, inflammatory, and infectious diseases [46]. IL-1β promotes invasiveness, including tumor angiogenesis, and also induces immune suppression in the host [38,47]. In pancreatic cancer cells, IL-1β mediates adhesion and invasion, and modulates chemoresistance by activating the NF-κB and ERK signaling pathways [41,48].

Finally, in order to investigate the effects of LICU on the vasculature, as well as the collagen production of PANC-1 tumor explants, we exposed the tumor explants to 2 h of LICU. Tumor explants were subsequently fixed and stained for CD31 and Collagen I. Our results (Figure 3) indicate that while IL-10, IL-12, IL-2, IL-4, IL-5, and IL-6 did not significantly increase following LICU treatment, the differential LICU effects on the secretion of cytokines suggest that further in vitro and in vivo animal studies are required to elucidate LICU's effects on tumor progression, while one cannot exclude co-administration with chemotherapeutic agents to enhance LICU's potential anti-tumorigenic effects.
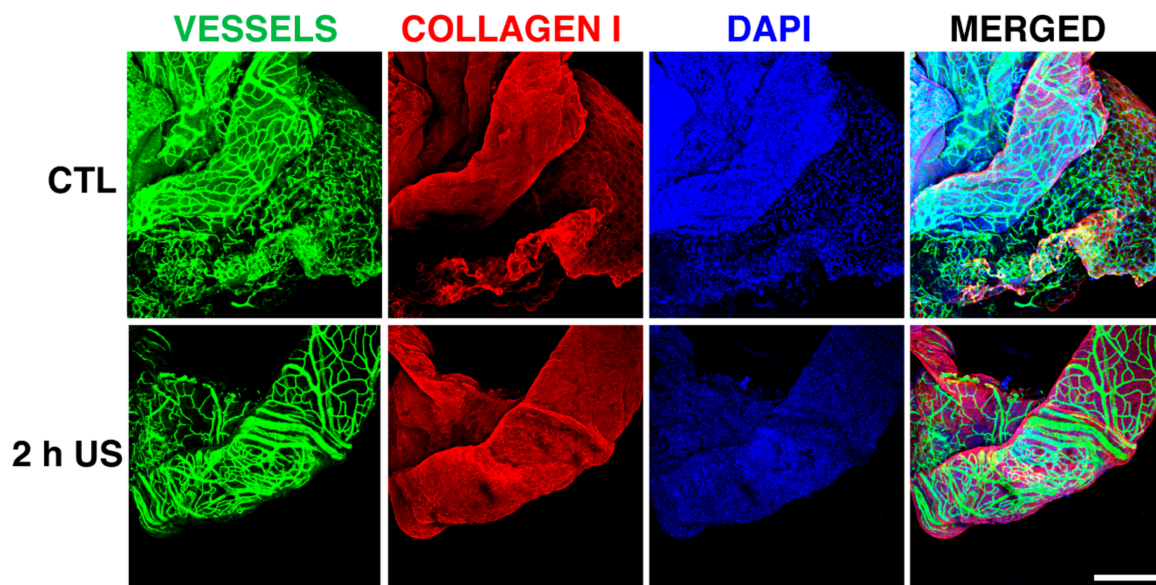

Figure 3. Confocal immunofluorescence images of mouse pancreatic tumor explants. Application of LICU for 2 h had no detectable effect on tumor vasculature (green) and collagen I (red) deposition. Cell nuclei were stained with DAPI (blue). Scale bar is 250 μm.

A novel observation in our study was that the tumor explants exhibited a homogeneous spatial behavior after the action of the ultrasonic standing waves was established within the chamber, with amplitudes that were spatially variable (Figure 1B). This finding describes for the first time the ability of cells and the extracellular matrix to provide a single-unit response to spatially variable acoustic waves above their different acoustic stimuli at different sample locations. The samples displayed in Figure 3 have a size of ~300 μm, covering an area of pressure amplitude pattern ~λ/4.

However, no differences were observed in the temporal evolution between different parts of each of these samples (in their vessels, DAPI, or collagen expression).

4. Conclusions

This work describes, for the first time, the effects that result from LICU being induced in tumor tissues. We demonstrate that application of LICU on mouse pancreatic tumor explants results in significant upregulation of the inflammatory cytokines IFN-γ, IL-β, and TNF-α. We also demonstrate the feasibility of the application of LICU for long times, which is approximately six times those applied by conventional LIPUS actuation without cell death in the limit condition of an infinite wave-train length for a LIPUS, i.e., LICU actuation.

Our observations describe, for the first time, the ability of cells and the extracellular matrix to provide a unitary response to acoustic waves with spatial variations in order of sample size. Ultrasonic waves that are strongly variable in space generate effects that are variable also in granulated material or suspensions of particles or cells associated with the gradient of radiation forces or other mechanisms that are acoustically induced. On the contrary, the continuity of the organic tissue and the continuous performance of LICU has probably generated a uniform response in our samples. It is a valuable finding from a strategic point of view, since it reduces the spatial restrictions of the acoustic wave, which often represents a technological problem.

In addition, we demonstrate the ability of the low intensity continuous ultrasound technology to stimulate a pro-inflammatory response in tissues and tumors. LICU can be further explored as a method to modulate the inflammatory response of tumors, with further potential for anti-tumorigenic effects, and can thus be considered as strategic tool for therapeutic purposes.

Author Contributions: Despina Bazou and Iciar Gonzalez performed most experiments and wrote the manuscript. Nir Maimon performed experiments. Lance Munn wrote the manuscript.

Conflicts of Interest: The authors declare no conflicts of interest.

References

1. Kristiansen, T.K.; Ryaby, J.P.; McCabe, J.; Frey, J.J.; Roe, L.R. Accelerated healing of distal radial fractures with the use of specific, low-intensity ultrasound: A multicenter, prospective, randomized, double-blind, placebo-controlled study. *J. Bone Jt. Surg. Am.* **1997**, *79*, 961–973. [CrossRef]

2. Busse, J.W.; Bhandari, M.; Kulkarni, A.V.; Tunks, E. The effect of low-intensity pulsed ultrasound therapy on time to fracture healing: A meta-analysis. *Can. Med. Assoc. J.* **2002**, *166*, 437–441.

3. Claes, L.; Willie, B. The enhancement of bone regeneration by ultrasound. *Prog. Biophys. Mol. Biol.* **2007**, *93*, 384–398. [CrossRef] [PubMed]

4. Mundi, R.; Petis, S.; Kaloty, R.; Shetty, V.; Bhandari, M. Low-intensity pulsed ultrasound: Fracture healing. *Indian J. Orthop.* **2009**, *43*, 132–140. [PubMed]

5. Xin, Z.; Lin, G.; Lei, H.; Lue, T.F.; Guo, Y. Clinical applications of low-intensity pulsed ultrasound and its potential role in urology. *Transl. Androl. Urol.* **2016**, *5*, 255–266. [CrossRef] [PubMed]

6. Wilson, S.R.; Greenbaum, L.D.; Goldberg, B.B. Contrast-Enhanced Ultrasound:What Is the Evidence and What Are the Obstacles? *Am. J. Roentgenol.* **2009**, *193*, 55–60. [CrossRef] [PubMed]

7. Helfield, B.; Chen, X.; Watkins, S.C.; Villanueva, F.S. Biophysical insight into mechanisms of sonoporation. *Proc. Natl. Acad. Sci. USA* **2016**, *113*, 9983–9988. [CrossRef] [PubMed]

8. El-Bialy, T.; Alhadlaq, A.; Wong, B.; Kucharski, C. Ultrasound effect on neural differentiation of gingival stem/progenitor cells. *Ann. Biomed. Eng.* **2014**, *42*, 1406–1412. [CrossRef] [PubMed]

9. Shiraishi, R.; Masaki, C.; Toshinaga, A.; Okinaga, T.; Nishihara, T.; Yamanaka, N.; Nakamoto, T.; Hosokawa, R. The effects of low-intensity pulsed ultrasound exposure on gingival cells. *J. Periodontol.* **2011**, *82*, 1498–1503. [CrossRef] [PubMed]

10. Harle, J.; Salih, V.; Mayia, F.; Knowles, J.C.; Olsen, I. Effects of ultrasound on the growth and function of bone and periodontal ligament cells in vitro. *Ultrasound Med. Biol.* **2001**, *27*, 579–586. [CrossRef]

11. Ren, L.; Yang, Z.; Song, J.; Wang, Z.; Deng, F.; Li, W. Involvement of p38 mapk pathway in low intensity pulsed ultrasound induced osteogenic differentiation of human periodontal ligament cells. *Ultrasonics* **2013**, *53*, 686–690. [CrossRef] [PubMed]

12. Hu, B.; Zhang, Y.; Zhou, J.; Li, J.; Deng, F.; Wang, Z.; Song, J. Low-intensity pulsed ultrasound stimulation facilitates osteogenic differentiation of human periodontal ligament cells. *PLoS ONE* **2014**, *9*, e95168. [CrossRef] [PubMed]

13. Dalla-Bona, D.A.; Tanaka, E.; Oka, H.; Yamano, E.; Kawai, N.; Miyauchi, M.; Takata, T.; Tanne, K. Effects of ultrasound on cementoblast metabolism in vitro. *Ultrasound Med. Biol.* **2006**, *32*, 943–948. [CrossRef] [PubMed]

14. Dalla-Bona, D.A.; Tanaka, E.; Inubushi, T.; Oka, H.; Ohta, A.; Okada, H.; Miyauchi, M.; Takata, T.; Tanne, K. Cementoblast response to low- and high-intensity ultrasound. *Arch. Oral. Biol.* **2008**, *53*, 318–323. [CrossRef] [PubMed]

15. Mukai, S.; Ito, H.; Nakagawa, Y.; Akiyama, H.; Miyamoto, M.; Nakamura, T. Transforming growth factor-beta1 mediates the effects of low-intensity pulsed ultrasound in chondrocytes. *Ultrasound Med. Biol.* **2005**, *31*, 1713–1721. [CrossRef] [PubMed]

16. Takeuchi, R.; Ryo, A.; Komitsu, N.; Mikuni-Takagaki, Y.; Fukui, A.; Takagi, Y.; Shiraishi, T.; Morishita, S.; Yamazaki, Y.; Kumagai, K.; et al. Low-intensity pulsed ultrasound activates the phosphatidylinositol 3 kinase/akt pathway and stimulates the growth of chondrocytes in three-dimensional cultures: A basic science study. *Arthritis Res. Ther.* **2008**, *10*, R77. [CrossRef] [PubMed]

17. Schumann, D.; Kujat, R.; Zellner, J.; Angele, M.K.; Nerlich, M.; Mayr, E.; Angele, P. Treatment of human mesenchymal stem cells with pulsed low intensity ultrasound enhances the chondrogenic phenotype in vitro. *Biorheology* **2006**, *43*, 431–443. [PubMed]

18. Angle, S.R.; Sena, K.; Sumner, D.R.; Virdi, A.S. Osteogenic differentiation of rat bone marrow stromal cells by various intensities of low-intensity pulsed ultrasound. *Ultrasonics* **2011**, *51*, 281–288. [CrossRef] [PubMed]

19. Nakao, J.; Fujii, Y.; Kusuyama, J.; Bandow, K.; Kakimoto, K.; Ohnishi, T.; Matsuguchi, T. Low-intensity pulsed ultrasound (LIPUS) inhibits LPS-induced inflammatory responses of osteoblasts through TLR4-MyD88 dissociation. *Bone* **2014**, *58*, 17–25. [CrossRef] [PubMed]

20. Lim, K.; Kim, J.; Seonwoo, H.; Park, S.H.; Choung, P.-H.; Chung, J.H. In vitro effects of low-intensity pulsed ultrasound stimulation on the osteogenic differentiation of human alveolar bone-derived mesenchymal stem cells for tooth tissue engineering. *Biomed. Res. Int.* **2013**, *2013*, 269724. [PubMed]

21. Al-Daghreer, S.; Doschak, M.; Sloan, A.J.; Major, P.W.; Heo, G.; Scurtescu, C.; Tsui, Y.Y.; El-Bialy, T. Effect of low-intensity pulsed ultrasound on orthodontically induced root resorption in beagle dogs. *Ultrasound Med. Biol.* **2014**, *40*, 1187–1196. [CrossRef] [PubMed]

22. Rego, E.B.; Inubushi, T.; Kawazoe, A.; Tanimoto, K.; Miyauchi, M.; Tanaka, E.; Takata, T.; Tanne, K. Ultrasound stimulation induces pge(2) synthesis promoting cementoblastic differentiation through ep2/ep4 receptor pathway. *Ultrasound Med. Biol.* **2010**, *36*, 907–915. [CrossRef] [PubMed]

23. Vaughan, N.M.; Grainger, J.; Bader, D.L.; Knight, M.M. The potential of pulsed low intensity ultrasound to stimulate chondrocytes matrix synthesis in agarose and monolayer cultures. *J. Med. Biol. Eng. Comput.* **2010**, *48*, 1215–1222. [CrossRef] [PubMed]

24. Buldakov, M.A.; Hassan, M.A.; Zhao, Q.L.; Feril, L.B., Jr.; Kudo, N.; Kondo, T.; Litvyakov, N.V.; Bolshakov, M.A.; Rostov, V.V.; Cherdyntseva, N.V.; et al. Influence of changing pulse repetition frequency on chemical and biological effects induced by low-intensity ultrasound in vitro. *Ultrason. Sonochem.* **2009**, *16*, 392–397. [CrossRef] [PubMed]

25. Yang, C.; Jiang, X.; Du, K.; Cai, Q. Effects of Low-Intensity Ultrasound on Cell Proliferation and Reproductivity. *Trans. Tianjin Univ.* **2016**, *22*, 125–131. [CrossRef]

26. Coussens, L.M.; Werb, Z. Inflammation and cancer. *Nature* **2002**, *420*, 860–867. [CrossRef] [PubMed]

27. Yarmolenko, P.S.; Moon, E.J.; Landon, C.; Manzoor, A.; Hochman, D.W.; Viglianti, B.L.; Dewhirst, M.W. Thresholds for thermal damage to normal tissues: An update. *Int. J. Hyperth.* **2011**, *27*, 320–343. [CrossRef] [PubMed]

28. Hurrell, A. Voltage to pressure conversion: Are you getting 'phased' by the problem? *J. Phys.* **2004**, *1*, 57–62. [CrossRef]

29. Nightingale, K.R.; Church, C.C.; Harris, G.; Wear, K.A.; Bailey, M.R.; Carson, P.L.; Jiang, H.; Sandstrom, K.L.; Szabo, T.L.; Ziskin, M.C. Conditionally Increased Acoustic Pressures in Nonfetal Diagnostic Ultrasound Examinations Without Contrast Agents: A Preliminary Assessment. *J. Ultrasound Med.* **2015**, *34*, 1–41. [CrossRef] [PubMed]

30. Ter Haar, G. Therapeutic ultrasound. *Eur. J. Ultrasound* **1999**, *9*, 3–9. [CrossRef]

31. Draper, D.O.; Castel, J.C.; Castel, D. Rate of temperature increase in human muscle during 1 mhz and 3 mhz continuous ultrasound. *J. Orthop. Sports Phys. Ther.* **1995**, *22*, 142–150. [CrossRef] [PubMed]

32. Jones, S.; Zhang, X.; Parsons, D.W.; Lin, J.C.; Leary, R.J.; Angenendt, P.; Mankoo, P.; Carter, H.; Kamiyama, H.; Jimeno, A.; et al. Core signaling pathways in human pancreatic cancers revealed by global genomic analyses. *Science* **2008**, *321*, 1801–1806. [CrossRef] [PubMed]

33. Fujioka, S.; Sclabas, G.M.; Schmidt, C.; Frederick, W.A.; Dong, Q.G.; Abbruzzese, J.L.; Evans, D.B.; Baker, C.; Chiao, P.J. Function of nuclear factor kappab in pancreatic cancer metastasis. *Clin. Cancer Res.* **2003**, *9*, 346–354. [PubMed]

34. Balkwill, F. Tumour necrosis factor and cancer. *Nat. Rev. Cancer* **2009**, *9*, 361–371. [CrossRef] [PubMed]

35. Furukawa, K.; Ohashi, T.; Haruki, K.; Fujiwara, Y.; Iida, T.; Shiba, H.; Uwagawa, T.; Kobayashi, H.; Yanaga, K. Combination treatment using adenovirus vector-mediated tumor necrosis factor-alpha gene transfer and a NF-kappaB inhibitor for pancreatic cancer in mice. *Cancer Lett.* **2011**, *306*, 92–98. [CrossRef] [PubMed]

36. Murugesan, S.R.; King, C.R.; Osborn, R.; Fairweather, W.R.; O'Reilly, E.M.; Thornton, M.O.; Wei, L.L. Combination of human tumor necrosis factor-alpha (hTNF-alpha) gene delivery with gemcitabine is effective in models of pancreatic cancer. *Cancer Gene Ther.* **2009**, *16*, 841–847. [CrossRef] [PubMed]

37. Egberts, J.H.; Cloosters, V.; Noack, A.; Schniewind, B.; Thon, L.; Klose, S.; Kettler, B.; von Forstner, C.; Kneitz, C.; Tepel, J.; et al. Anti-tumor necrosis factor therapy inhibits pancreatic tumor growth and metastasis. *Cancer Res.* **2008**, *68*, 1443–1450. [CrossRef] [PubMed]

38. Maier, H.J.; Schmidt-Strassburger, U.; Huber, M.A.; Wiedemann, E.M.; Beug, H.; Wirth, T. NF-kappaB promotes epithelial-mesenchymal transition, migration and invasion of pancreatic carcinoma cells. *Cancer Lett.* **2010**, *295*, 214–228. [CrossRef] [PubMed]

39. Apte, M.V.; Park, S.; Phillips, P.A.; Santucci, N.; Goldstein, D.; Kumar, R.K.; Ramm, G.A.; Buchler, M.; Friess, H.; McCarroll, J.A.; et al. Desmoplastic reaction in pancreatic cancer: Role of pancreatic stellate cells. *Pancreas* **2004**, *29*, 179–187. [CrossRef] [PubMed]

40. Bachem, M.G.; Schünemann, M.; Ramadani, M.; Siech, M.; Beger, H.; Buck, A.; Zhou, S.; Schmid-Kotsas, A.; Adler, G. Pancreatic carcinoma cells induce fibrosis by stimulating proliferation and matrix synthesis of stellate cells. *Gastroenterology* **2005**, *128*, 907–921. [CrossRef] [PubMed]

41. Muerkoster, S.; Wegehenkel, K.; Arlt, A.; Witt, M.; Sipos, B.; Kruse, M.L.; Sebens, T.; Klöppel, G.; Kalthoff, H.; Fölsch, U.R.; et al. Tumor stroma interactions induce chemoresistance in pancreatic ductal carcinoma cells involving increased secretion and paracrine effects of nitric oxide and interleukin-1beta. *Cancer Res.* **2004**, *64*, 1331–1337. [CrossRef] [PubMed]

42. Baumert, J.T.; Sparmann, G.; Emmrich, J.; Liebe, S.; Jaster, R. Inhibitory effects of interferons on pancreatic stellate cell activation. *World J. Gastroenterol.* **2006**, *12*, 896–901. [CrossRef] [PubMed]

43. Nukui, Y.; Picozzi, V.J.; Traverso, L.W. Interferon-based adjuvant chemoradiation therapy improves survival after pancreaticoduodenectomy for pancreatic adenocarcinoma. *Am. J. Surg.* **2000**, *179*, 367–371. [CrossRef]

44. Picozzi, V.J.; Kozarek, R.A.; Traverso, L.W. Interferon-based adjuvant chemoradiation therapy after pancreaticoduodenectomy for pancreatic adenocarcinoma. *Am. J. Surg.* **2003**, *185*, 476–480. [CrossRef]

45. Landvik, N.E.; Hart, K.; Skaug, V.; Stangeland, L.B.; Haugen, A.; Zienolddiny, S. A specific interleukin-1B haplotype correlates with high levels of IL1B mRNA in the lung and increased risk of non-small cell lung cancer. *Carcinogenesis* **2009**, *30*, 1186–1192. [CrossRef] [PubMed]

46. Aksentijevich, I.; Masters, S.L.; Ferguson, P.J.; Dancey, P.; Frenkel, J.; Van Royen-Kerkhoff, A.; Laxer, R.; Tedgård, U.; Cowen, E.W.; Pham, T.H.; et al. An autoinflammatory disease with deficiency of the interleukin-1-receptor antagonist. *N. Engl. J. Med.* **2009**, *360*, 2426–2437. [CrossRef] [PubMed]

47. Voronov, E.; Carmi, Y.; Apte, R.N. The role IL-1 in tumor-mediated angiogenesis. *Front. Physiol.* **2014**, *5*, 114. [CrossRef] [PubMed]

48. Angst, E.; Reber, H.A.; Hines, O.J.; Eibl, G. Mononuclear cell-derived interleukin-1 beta confers chemoresistance in pancreatic cancer cells by upregulation of cyclooxygenase-2. *Surgery* **2008**, *144*, 57–65. [CrossRef] [PubMed]